Greatly Facilitated Oxygen Vacancy Formation in Ceria Nanocrystallites

Electronic Supplementary Information

Annapaola Migani,*[,§] Georgi N. Vayssilov[†] Stefan T. Bromley,[§,‡]
Francesc Illas[§,‡] and Konstantin M. Neyman*[,§,‡]

IQTCUB & Departament de Química Física, Universitat de Barcelona, 08028 Barcelona, Spain, Faculty of Chemistry, University of Sofia, 1126 Sofia, Bulgaria, Institució Catalana de Recerca i Estudis Avançats (ICREA), 08010 Barcelona, Spain

CeO_2 nanoparticle models

The design of adequate representative CeO_2 nanoparticle (NP) models is crucial for the reliability of calculated formation energies of oxygen vacancies. The potential energy surface (PES) even for fairly small ceria clusters is much too complex to be explored completely using high-level quantum-mechanical schemes. Thus, for choosing a proper shape and geometry of the model NPs one has to resort to molecular modelling using computationally efficient empirically parameterised methods, which allows for the identification of low-energy structures to be refined by density functional calculations.[1] Following studies on other similarly sized oxide clusters[2] we used the basin hopping approach[3] based on interatomic potentials (IP) to explore the PES of isomers for the $Ce_{21}O_{42}$, and $Ce_{40}O_{80}$ stoichiometric NPs. At each basin hopping step the positions of the Ce^{4+} and O^{2-} ions are randomised and the resulting structure optimised to the nearest local minimum. Each new minimised configuration is then accepted or not dependent on its energy with respect to a Monte Carlo criterion. In this way the geometries are ensured to be close to the global energetic minima at these particular sizes as the method tends towards lower energy structures. The geometry of $Ce_{80}O_{160}$ is constructed consistently with the low-energy structure obtained with basin hopping approach for $Ce_{40}O_{80}$, by removing five corners Ce from the previously reported[4] non-stoichiometric octahedral bulk-cut $Ce_{85}O_{160}$ NP.

In the global optimisation calculation, the stoichiometric NPs include the Ce^{4+} and O^{2-} ionic species. The IPs consist of a long-range Coulombic term and a short-range term in the form of a Buckingham function. A shell model is used to account for the ion polarisability induced by the electric field produced by all other ions.[5] Due to the often severe disruption of ionic positions a repulsive short range term was added to each potential in order to avoid

[§] Universitat de Barcelona.
[†] University of Sofia.
[‡] ICREA.

spurious ionic coalescence, which may occur due to the form of the interatomic potentials at very short distances. The addition of such terms was verified to have no effect with respect to the optimised energies and structures of the clusters using the bare form. In order to carefully sample the PES we employed numerous basin-hopping runs of approximately 250 000 steps each from different starting structures (both randomised and hand-selected). Whenever a new low-energy nanocluster was found its structure was then also used as the seed for a subsequent basin-hopping run to help sampling of the nearby part of the PES.

In the basin hopping approach only the Coulombic and short-range interactions were taken into account. In a subsequent step, the first ten lowest energy isomers for each NP are refined by including the shell model. The lowest energy isomer obtained in this way corresponds to the geometry employed in the density functional calculations of the pristine (without O vacancies) NP. Short-range potential parameters describing the Ce-O and O-O interactions and the Ce^{4+} shell model parameters are taken from Ref. 6. The O^{2-} shell model parameters are taken from Ref. 7.

These bulk-parameterised IPs (with the addition of the Ce^{3+}-O^{2-} interatomic term) have been employed to compute stoichiometric and reduced ceria surfaces,[6,9] CeO_2-ZrO_2 bulk[7] and surface[8] solutions, and large CeO_2 NPs.[10] Moreover, they were also used in a simulated annealing study[11] to search for the global minimum of stoichiometric clusters of increasing size Ce_nO_{2n} (n=2-10, n=50). Applicability of the IPs to smaller reduced ceria NPs featuring bulk-like atomic structure was also previously validated by us against DFT+U data:[12] their sufficient reliability for the present work is justified by good agreement of structural parameters and relative energy stability for different Ce^{3+}/Ce^{4+} cationic orderings of the $Ce_{19}O_{32}$ NP at the IP and DFT+U levels. The same energetic ordering of the lowest-energy isomers of $Ce_{19}O_{32}$ generated by basin-hopping and reproduced at the DFT+U level[4,13] also supports usage of the IP scheme in global optimisation.

Density functional calculations

VASP calculations were performed within the DFT+U approach, using the PW91 exchange-correlation (*xc*) functional[14] and U = 4 eV [referred to hereafter as PW91+4] that is close to the U values commonly employed in calculations of ceria.[15] For the CeO_2(111) surface calculations we employed a (2×2) surface unit cell, twelve atomic layers and a 1.2 nm vacuum. All atomic coordinates were optimized, both in the stoichiometric and defective structures. The $Ce_{16}O_{32}$ step on the (6×4) CeO_2(111) surface unit cell of nine atomic layers was obtained by deleting two rows of outermost cerium atoms and three rows of surface and

one row of subsurface O atoms (Fig. S1). One of the two steps exposes arrangement of the {100} plane with two-coordinated O atoms (see black circle in Fig. S1). In the stepped surface calculations of stoichiometric and defective structures the first four outermost atomic layers were relaxed and the remaining ones were kept fixed at the experimental bulk lattice parameter. As for the clusters, only Γ-point calculations were performed.

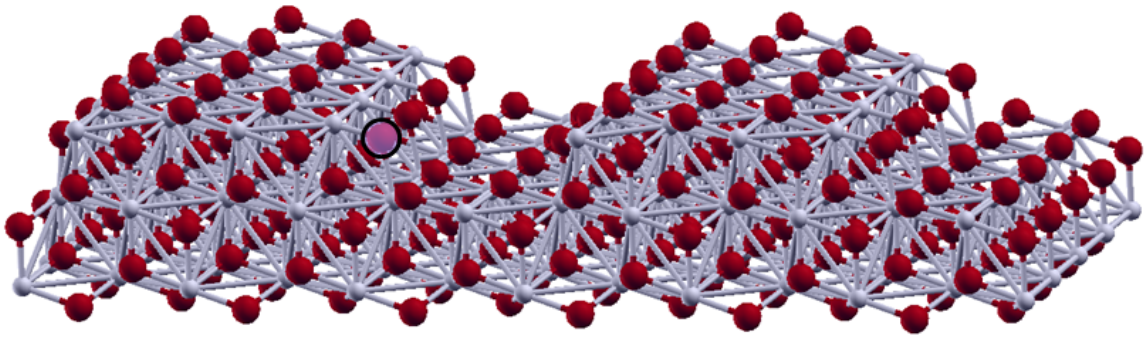

Fig. S1. Model of the step edge exposing a {100} facet with two-coordinated O atoms.

In the following we compare some of our data with those calculated for a CeO_2(111) surface model within another gradient-corrected approximation (GGA) employing the PBE *xc*,[16] in the PBE+4.5 form.[17] Probably more important is our comparison with the reference data for CeO_2(111) surface calculated with the hybrid HSE06 method,[18] known to provide properly localized solutions for reduced ceria without the need of further corrections.[17]

The HSE06 values discussed in the main text for the O vacancy ($V_O^{\cdot\cdot}$) formation energy (E_f) in $Ce_{21}O_{42}$ (Fig. 1) were obtained for both the pristine $Ce_{21}O_{42}$ and all defective $Ce_{21}O_{41}$ species under scrutiny that were *fixed* at the geometries optimized at the PW91+4 level. This resulted in the same positions of the Ce^{3+} pairs in the corresponding PW91+4 and HSE06 calculations. Benchmark HSE06 geometry optimization for the $V_O^{\cdot\cdot}$ characterized by E_f^{PW91+4} = 1.82 eV (Fig. 1) resulted in a lowering of the total HSE06 energy for the pristine $Ce_{21}O_{42}$ by 1.44 eV and for its congener $Ce_{21}O_{41}$ with the depleted O atom, by 1.36 eV. Based on this estimation, the somewhat non-uniform HSE06 relaxation of the regular and the $V_O^{\cdot\cdot}$ structures would increase the E_f^{HSE06} values listed in Fig. 1 by about 0.08 eV. On the other hand, our tests for NPs reveal that the $E_f^{PBE+4.5}$ values are systematically smaller than the corresponding E_f^{PW91+4} ones, by 0.17 eV (averaged over 12 values for a $Ce_{30}O_{60}$ NP, not presented). Estimated difference between the E_f^{PW91+4} and E_f^{HSE06} energies of single $V_O^{\cdot\cdot}$ in $Ce_{21}O_{42}$ is 0.42 eV (averaged over 8 values, Fig. 1). These our estimations give an overall deviation of

$E_f^{PBE+4.5}$ values from E_f^{HSE06} ones in NPs of 0.59 eV, which after adding 0.08 eV of the missing geometry relaxation in our HSE06 calculations is in almost quantitative agreement with results by Ganduglia-Pirovano et al.[17] (i.e. that formation of $V_O^{\cdot\cdot}$ on the $CeO_2(111)$ surface at the PBE+4.5 level requires 0.78 eV less energy than that in the HSE06 approach).

For estimation of $V_O^{\cdot\cdot}$ formation energies at a more sophisticated hybrid level HSE06 in larger NPs $Ce_{40}O_{80}$ and $Ce_{80}O_{160}$, still too demanding for direct calculations, we used the linear correlation $E_f^{HSE06}(eV) = 1.08\ E_f^{PW91+4} + 0.27$ ($R^2 = 0.98$), which we obtained for the $Ce_{21}O_{42}/Ce_{21}O_{41}$ models.

The common (absolute) energy scale for the DOS plot in Fig. 4 is obtained by adjusting for each NP the Kohn-Sham (KS) energies to the vacuum potential value (E_{vac}) in the direction normal to the {100} facet, where the lowest-energy $V_O^{\cdot\cdot}$ is created. The KS energies in Fig. S2 are adjusted in the same way, but by the E_{vac} normal to the (111) surface.

Electrostatic field values $V(Ce^{4+})$ and $V(O^{2-})$ at the nuclei of Ce^{4+} and O^{2-} ions, respectively, in stoichiometric Ce_nO_{2n} NPs (n = 21, 40, 80) are those from the VASP output, adjusted for comparison to the vacuum E_{vac} values as stated above. These values govern in each NP the choice of the O atom to be abstracted and two Ce^{4+} cations to be reduced to Ce^{3+} (with localized $4f^1$ electron), which results in the lowest E_f values. Indeed, in all three NPs the O^{2-} anion and Ce^{4+} cations involved in the electron transfer (excitation) process $O^{2-} + 2\ Ce^{4+} \rightarrow O + 2\ Ce^{3+}$ leading to the lowest E_f^{PW91+4} (Fig. 1, Table S1) are characterized, respectively, by the least negative $V(O^{2-})$ and the most negative □$(Ce^{4+}) = [V(Ce_1^{4+}) + V(Ce_2^{4+})]/2$ values within the set computed for each NP (Table S1). This affects the energies of the O 2p orbitals, ε(O 2p), and Ce 4f orbitals, $\varepsilon(Ce_1\ 4f)$ and $\varepsilon(Ce_2\ 4f)$, so that the orbitals of the O^{2-} anion experiencing the least negative electrostatic field are among the highest occupied molecular orbitals (MO). Concomitantly, the orbitals localised on the Ce^{4+} cations at the positions most stabilized by the field are lowered in energy and thus contribute to the lowest unoccupied MOs (see partial DOS of the O^{2-} anion and Ce^{4+} cations, Fig. 4). Moreover, as shown in Table S1, the change of the lowest E_f value with the particle size correlates with the variation of the electrostatic potential. For comparison, we include our computed $V(O^{2-})$ and $V(Ce^{4+})$ values at a subsurface O atom and two Ce^{4+} cations second-neighbors to (one in the plane above and the other in the plane below) the O position in the pristine $CeO_2(111)$ slab model.

Table S1. Electrostatic field at the nuclei of the O^{2-} anion, $V(O^{2-})$, and two Ce^{4+} cations, $V(Ce_1^{4+})$ and $V(Ce_2^{4+})$ for $V_O^{\cdot\cdot}$ with lowest E_f^{PW91+4} in the three Ce_nO_{2n} NPs. □(Ce^{4+}) = $[V(Ce_1^{4+}) + V(Ce_2^{4+})]/2$, $\Delta V = V(O^{2-})$ – □(Ce^{4+}). Deviations of $V(O^{2-})$ and □(Ce^{4+}) from the least negative O^{2-} and most negative Ce^{4+} values, respectively, in parentheses. Highest and lowest orbital energies of the O^{2-} anion, ε(O 2p), and two Ce^{4+} cations, $\varepsilon(Ce_1\ 4f)$ and $\varepsilon(Ce_2\ 4f)$, respectively, and excitation energy $2\Delta\varepsilon \equiv \Delta\varepsilon_1 + \Delta\varepsilon_2 = [\varepsilon(Ce_1\ 4f) - \varepsilon(O\ 2p)] + [\varepsilon(Ce_2\ 4f) - \varepsilon(O\ 2p)]$. Reference data for $CeO_2(111)$ slab model are also shown. All energy values are in eV.

System	$V(O^{2-})$	$V(Ce_1^{4+})$	$V(Ce_2^{4+})$	□(Ce^{4+})	ΔV	ε(O 2p)	$\varepsilon(Ce_1\ 4f)$	$\varepsilon(Ce_2\ 4f)$	2Δε	E_f^{PW91+4}
$Ce_{21}O_{42}$	-79.77 (-0.10)	-93.01	-93.01	-93.01 (+0.40)	13.24	-6.14	-3.92	-3.92	4.44	2.12
	-79.77 (-0.10)	-93.01	-93.01	-93.01 (+0.40)	13.24	-6.14	-3.92	-3.92	4.44	2.04
	-79.77 (-0.10)	-93.27	-93.27	-93.27 (+0.10)	13.51	-6.14[b]	-4.07[b]	-4.07[b]	4.14	1.67
$Ce_{40}O_{80}$	-79.35 (+0.00)	-93.15	-93.13	-93.14 (+0.02)	13.79	-5.64[b]	-3.99[b]	-4.12[b]	3.18	0.83
	-79.35 (+0.00)	-93.13	-93.13	-93.13 (+0.03)	13.77	-5.64	-4.12	-4.12	3.05	0.80
$Ce_{80}O_{160}$	-79.34 (-0.11)	-93.62	-93.27	-93.44 (+0.18)	14.10	-5.65[b]	-4.08[b]	-4.56[b]	2.67	0.46
$CeO_2(111)$	-80.50 (-0.52)	-93.33	-93.27	-93.30 (+0.03)	12.79	-6.66[b]	-4.29[b]	-4.28[b]	4.76	2.60[a]

[a]E_f^{PW91+5} for the slab model with (2×2) surface unit cell and nine atomic layers from Ref.[19].
[b]Red, and blue arrows in Fig. 4 and Fig. S2.

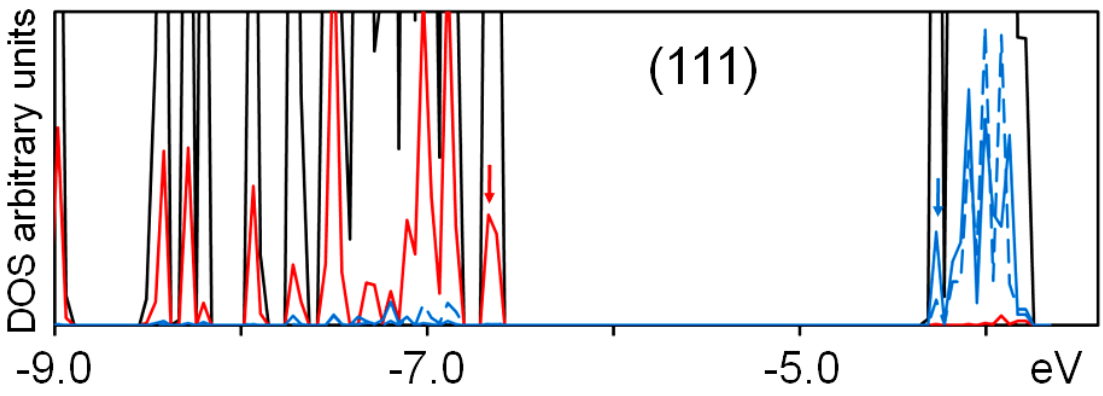

Fig. S2. Total (black line) and partial density of states (DOS) of the $CeO_2(111)$ surface in absolute energy scale (cf. Fig. 4). Red – 2p DOS of atoms O removed with the lowest E_f according to Ref. 17, blue – 4f DOS of two Ce^{4+} ions reduced by two electrons of the O^{2-} during depletion. Arrows mark boundary states dominated by O (red) and Ce (blue) atoms involved in the electron transfer that would accompany formation of the chosen $V_O^{\cdot\cdot}$.

References

1 S. T. Bromley, I. D. R. Moreira, K. M. Neyman and F. Illas, *Chem. Soc. Rev.*, 2009, **38**, 2657.

2 S. T. Bromley and E. Flikkema, *Phys. Rev. Lett.*, 2005, **95**.

3 D. J. Wales and J. P. K. Doye, *J. Phys. Chem. A*, 1997, **101**, 5111.

4 C. Loschen, S. T. Bromley, K. M. Neyman and F. Illas, *J. Phys. Chem. C*, 2007, **111**, 10142.

5 B. G. Dick and A. W. Overhauser, *Phys. Rev.*, 1958, **112**, 90.

6 T. X. T. Sayle, S. C. Parker and C. R. A. Catlow, *J. Chem. Soc., Chem. Comm.*, 1992, 977.

7 G. Balducci, J. Kaspar, P. Fornasiero, M. Graziani, M. S. Islam and J. D. Gale, *J. Phys. Chem. B*, 1997, **101**, 1750.

8 G. Balducci, J. Kaspar, P. Fornasiero, M. Graziani and M. S. Islam, *J. Phys. Chem. B*, 1998, **102**, 557.

9 J. C. Conesa, *Surf. Sci.*, 1995, **339**, 337.

10 T. X. T. Sayle, S. C. Parker and D. C. Sayle, *Chem. Comm.*, 2004, 2438.

11 H. Cordatos, D. Ford and R. J. Gorte, *J. Phys. Chem.*, 1996, **100**, 18128.

12 A. Migani, K. M. Neyman, F. Illas and S. T. Bromley, *J. Chem. Phys.*, 2009, **131**, 064701.

13 C. Loschen, A. Migani, S. T. Bromley, F. Illas and K. M. Neyman, *Phys. Chem. Chem. Phys.*, 2008, **10**, 5730.

14 J. P. Perdew, J. A. Chevary, S. H. Vosko, K. A. Jackson, M. R. Pederson, D. J. Singh and C. Fiolhais, *Phys. Rev. B*, 1992, **46**, 6671; J. P. Perdew, J. A. Chevary, S. H. Vosko, K. A. Jackson, M. R. Pederson, D. J. Singh and C. Fiolhais, *Phys. Rev. B*, 1993, **48**, 4978.

15 C. Loschen, J. Carrasco, K. M. Neyman and F. Illas, *Phys. Rev. B*, 2007, **75**, 035115.

16 J. P. Perdew, K. Burke and M. Ernzerhof, *Phys. Rev. Lett.*, 1996, **77**, 3865.

17 M. V. J. Ganduglia-Pirovano, L. F. Da Silva and J. Sauer, *Phys. Rev. Lett.*, 2009, **102**, 026101.

18 A. V. Krukau, O. A. Vydrov, A. F. Izmaylov and G. E. Scuseria, *J. Chem. Phys.*, 2006, **125**, 224106.

19 M. Nolan, J. E. Fearon and G. W. Watson, *Sol. St. Ionics*, 2006, **177**, 3069.